



## Measurement of the $t\bar{t}$ differential cross section, $d\sigma/dM_{t\bar{t}}$ , in $2.7 fb^{-1}$ of CDF II Data

The CDF Collaboration  
URL <http://www-cdf.fnal.gov>  
(Dated: November 11, 2008)

We present a measurement of the  $t\bar{t}$  differential cross section,  $d\sigma/dM_{t\bar{t}}$ , at  $\sqrt{s} = 1.96$  TeV using  $\sim 2.7 fb^{-1}$  of data collected with the CDF II Detector at the Fermilab Tevatron. We select events in the  $W + \geq 4$  jets sample with displaced secondary vertices from jets with heavy-flavor decays. We use an *in-situ* calibration of the jet energy scale to reduce the systematic uncertainties and a regularized unfolding technique to correct the reconstructed invariant mass distribution back to the true distribution. We see no evidence of inconsistency with the Standard Model, with an observed p-value of 0.28. We set limits on  $\kappa/M_{Pl}$  in the Randall-Sundrum model by looking for gravitons which decays to top quarks.

## I. INTRODUCTION

The Standard Model (SM) of particle physics is a remarkably successful theory of the strong and electroweak interactions at the energy scales which have been experimentally tested thus far. However the SM remains an incomplete theory. In the SM the Higgs boson is responsible for electroweak symmetry breaking (EWSB) and the generation of fermion masses. The SM prefers a light Higgs boson [1] well within the reach of current experiments, but it has not yet been found, opening the possibility for a beyond the SM (BSM) mechanism of EWSB. Because the top quark is the only known fermion with a mass near the EWSB scale, it plays a special role in many BSM theories of EWSB. In these models the top quark can play either a direct or an indirect role in the EWSB. In models with top condensation such as technicolor and topcolor models, the role of the SM Higgs boson is filled by a composite particle which is a bound state of top quarks [2]. These models predict additional heavy gauge boson which couple strongly to top quarks. The gauge bosons can be either color singlets, such as a  $Z'$  boson [3], or color octets, such as colorons [4] or axigluons [5]. The color-singlet  $Z'$  bosons generally produce narrow resonances in the  $M_{t\bar{t}}$  spectrum, without interference with the SM process. However the color octet processes do interfere with the SM strong interaction, causing distortions to the  $M_{t\bar{t}}$  spectrum that are not simple resonances. The two Higgs doublet and minimal supersymmetric models are examples of models without top quark condensation. In these models, the pseudoscalar Higgs boson may couple strongly to top quarks, causing a peak-dip structure in the  $M_{t\bar{t}}$  spectrum. [6]

The unification of all of the fundamental forces, including gravity, requires more exotic physics beyond the SM. The fundamental problem which must be addressed is why the force of gravity is so weak as compared to the other forces - this is the hierarchy problem. In physics models with extra dimensions the structure of space-time accounts for the extreme weakness of gravity. In the Randall-Sundrum (RS) model a single warped extra dimension accounts for the observed hierarchy [7]. Kaluza-Klein (KK) gravitons which propagate in the bulk space and decay to top quarks would be seen as a series of resonances in the  $M_{t\bar{t}}$  spectrum.

The study of the  $M_{t\bar{t}}$  spectrum is sensitive to a very broad class of models which produce distortions to the spectrum ranging from narrow resonances to broad interferences [8]. In a previous version of this analysis, completed with  $1.9 \text{ fb}^{-1}$  of CDF II data [9] we found no evidence for physics beyond the SM, but were limited in our sensitivity by large systematic uncertainties. For this updated analysis we implement a calibration of the jet energy scale (JES) which significantly reduces the systematic uncertainties and improves our sensitivity to physics beyond the SM.

## II. DEFINITION

We measure  $d\sigma/dM_{t\bar{t}}$ , as defined by:

$$\frac{d\sigma^i}{dM_{t\bar{t}}} = \frac{N_i - N_i^{bkg}}{\mathcal{A}_i \int \mathcal{L} \Delta_{M_{t\bar{t}}}^i}$$

where  $N_i$  is the number of events observed in each bin,  $N_i^{bkg}$  is the predicted number of background events and  $\mathcal{A}_i$  is the acceptance in bin  $i$ ;  $\Delta_{M_{t\bar{t}}}^i$  is the width of bin  $i$ ; and  $\int \mathcal{L}$  is the integrated luminosity. We divide the  $M_{t\bar{t}}$  distribution into 9 bins: 0-350, 350-400, 400-450, 450-500, 500-550, 550-600, 600-700, 700-800 and 800-1400  $\text{GeV}/c^2$ .

## III. DATA SAMPLE & EVENT SELECTION

We use  $\sim 2.7 \text{ fb}^{-1}$  of CDF II data, collected between March 2002 and April 2008. The data are collected with an inclusive lepton trigger, which requires an electron with  $E_T > 18 \text{ GeV}$  or a muon with  $p_T > 18 \text{ GeV}/c$ . The offline selection requires a lepton with  $E_T > 20 \text{ GeV}$  ( $p_T > 20 \text{ GeV}/c$  for

muons), missing transverse energy greater than  $20 \text{ GeV}$  and at least 4 jets with  $E_T > 20 \text{ GeV}$ . To further reduce the backgrounds, we require at least one jet with an identified displaced secondary vertex, from a heavy-flavor decay. We identify these jets as  $b$ -jets (“ $b$ -tagged”) from the decay  $t \rightarrow Wb$ . With this event selection, we observe 650 total events. The CDF II detector is described in detail elsewhere [13].

The calibration of JES relies upon a fit of the invariant mass distribution of the dijets from the hadronically decaying  $W$  boson,  $M_{jj}$ . We identify the daughters of the  $W$  boson as follows: for events with 2  $b$ -tags we assume the 2 untagged jets (of the leading 4 jets in the event) as the daughters of the hadronically decaying  $W$ . For events with a single  $b$ -tag we find the pair of untagged jets among the leading 4 that has an invariant mass which is most consistent with the  $W$  boson mass.

We reconstruct the invariant mass of the  $t\bar{t}$  pair by combining the 4-vectors of the 4 leading jets, lepton and missing transverse energy. This reconstructed  $M_{t\bar{t}}$  distribution is distorted from the true distribution by detector effects, including jet and missing energy resolution, and our geometric and kinematic acceptance. We correct for these effects by using a regularized unfolding technique, Singular Value Decomposition (SVD) unfolding [15].

## IV. ANALYSIS OVERVIEW

In this section we present details for each component of the analysis. In Section IV A we present the estimation of the SM backgrounds. In Section IV B we describe the details of the JES calibration. After calibrating the JES we unfold the background-subtracted  $M_{t\bar{t}}$  distribution as described in Section IV C. The number of events in the JES-dependent unfolded  $M_{t\bar{t}}$  distribution is then divided by the product of the acceptance, integrated luminosity and bin width - the denominator of Equation 1 - to obtain the measured  $d\sigma/dM_{t\bar{t}}$ . We describe the calculation of the denominator and its dependence on the JES calibration in Section IV D.

### A. Backgrounds

The  $t\bar{t}$  signature described in Section III can be mimicked by several Standard Model processes, including diboson production, single top production, and  $W$ +jets production. The least-well theoretically constrained of these processes is the  $W$ +jets production cross section, due to the difficulties of high-order QCD calculations. We use a background estimation, described previously in [16], which uses the theoretically well-known processes to constrain the data sample composition. This estimation was repeated in the  $2.7 \text{ fb}^{-1}$  dataset in a separate analysis [17].

The calculation of the expected number of events from the electroweak processes – diboson,  $Z$ +jets, single top – is straightforward. We calculate an acceptance for each process, analogously to the  $t\bar{t}$  acceptance described in Section IV D, and obtain the total number of expected events according to  $N = \sigma \mathcal{A} \int \mathcal{L}$ . These processes, with the exception of single-top and  $Z$ +jets, are modeled with a PYTHIA Monte Carlo simulation. The single-top background is modeled by a MADEVENT [18] Monte Carlo simulation which is showered with PYTHIA, the  $Z$ +jets background is modeled by an ALPGEN [19] Monte Carlo simulation which is showered by PYTHIA. These backgrounds are small for our event selection.

The largest component of the background is  $W$ +jets production. We separate the tagged heavy flavor component of the  $W$ +jets background from the tagged light flavor component. We assume that while the absolute cross section for heavy flavor production is very sensitive to higher order corrections, that the fraction is not. Therefore we calculate the fraction of  $W$ +jets events with bottom and charm content in an ALPGEN Monte Carlo simulation with PYTHIA showering, and obtain the absolute normalization from the number of  $W$ +jets events before the tagging selection (“pretag”) in the data. The number of expected  $W$ +heavy flavor events we obtain is corrected for differences in heavy flavor content and tagging efficiency in data and Monte Carlo.

The QCD background expectation is obtained by fitting the shape of the missing  $E_T$  distribution in data. Events with no real  $W$  will generally have low missing energy because of the absence of

CDF II Preliminary, $\int \mathcal{L} \approx 2.7 \text{ fb}^{-1}$		
Process	4 jets	$\geq 5$ jets
Wbb	$32.3 \pm 10.5$	$6.5 \pm 2.5$
Wcc	$16.8 \pm 5.6$	$3.6 \pm 1.4$
Wc	$8.9 \pm 2.9$	$1.5 \pm 0.6$
Mistags	$18.9 \pm 4.8$	$3.5 \pm 1.6$
Non-W	$20.9 \pm 17.5$	$6.4 \pm 6.0$
WW	$3.5 \pm 0.5$	$1.0 \pm 0.1$
WZ	$1.2 \pm 0.1$	$0.3 \pm 0.0$
ZZ	$0.3 \pm 0.0$	$0.1 \pm 0.0$
Z+jets	$3.3 \pm 0.4$	$0.7 \pm 0.1$
Single Top (s-channel)	$2.8 \pm 0.3$	$0.6 \pm 0.1$
Single Top (t-channel)	$2.8 \pm 0.2$	$0.4 \pm 0.0$
$t\bar{t}$ (6.7pb)	$358.6 \pm 49.7$	$121.5 \pm 16.8$
Total Prediction	$470.3 \pm 56.5$	$145.9 \pm 18.5$
Observed	494	156

TABLE I: Summary of sample composition. [17]

a high  $p_T$  neutrino. The fit allows an extrapolation from the low missing energy side band to the signal region, with missing  $E_T$  greater than 20 GeV.

The remainder of the  $W$ +jets background in the tagged data is a result of the misidentification of light flavor jets as heavy flavor, or “mistags”. To first order, the mistags may be modeled by events in which the secondary vertex position corresponds to a negative decay length. The rate of negative tags is parameterized as a function of jet energy, jet  $\eta$ , number of tracks, number of  $z$ -vertices, primary vertex position and the sum of the event transverse energy in a mistag matrix. The sum of probabilities from the matrix on all jets in the event yields the number of negative tags. This number is corrected for an asymmetry in the negative versus positive decay probability for mistags and real heavy flavor content of the mistag matrix. The predicted number of  $W$ +light flavor events is then the number of negative tags times the fraction of  $W$ +light flavor events in the  $W$ +jets sample.

The composition of our data sample is summarized in Table I. The “ $M_{t\bar{t}}$ ” and  $M_{jj}$  distributions of the backgrounds are modeled with the same Monte Carlo or data samples used in calculation of the absolute normalizations of the the relevant processes. The uncertainty on the overall normalization of the backgrounds includes the uncertainty due to the JES. The background shapes do not vary appreciably with respect to variations in the JES and are kept constant in this analysis.

## B. Jet Energy Scale Calibration

Like any analysis that relies heavily on jet information, the uncertainty on the JES is a dominant source of systematic uncertainty in this analysis. We have previously completed an analysis of  $d\sigma/dM_{t\bar{t}}$  with  $1.9 \text{ fb}^{-1}$  of data [9], where the JES uncertainty was the largest source of systematic uncertainty, followed by the uncertainty on the Parton Distribution Function (PDF) used in the Monte Carlo simulation. In order to constrain the JES uncertainty we use a technique similar to that developed for use in the analysis of the top quark mass [10].

The derivation of the nominal jet energy scale at CDF is described elsewhere [11]. Fig 1 shows the total jet energy scale uncertainty as a function of corrected jet  $p_T$ . We measure the quantity  $\Delta_{JES}$ , which is the deviation from the nominal JES ( $\Delta_{JES} = 0$ ) in units of the nominal jet energy scale uncertainty,  $\sigma_{JES}$ , as shown in Figure 1. The differential cross section depends on the value of  $\Delta_{JES}$ , as will be explained in detail in the following sections. The measured  $d\sigma/dM_{t\bar{t}}$  will be calculated at the value of  $\Delta_{JES}$  measured in the data,  $\Delta_{JES}^{data}$ , with the uncertainty on  $\Delta_{JES}^{data}$  as an additional source of statistical uncertainty.

We reconstruct the invariant mass of the hadronically decaying  $W$  boson in the data,  $M_{jj}$ , and

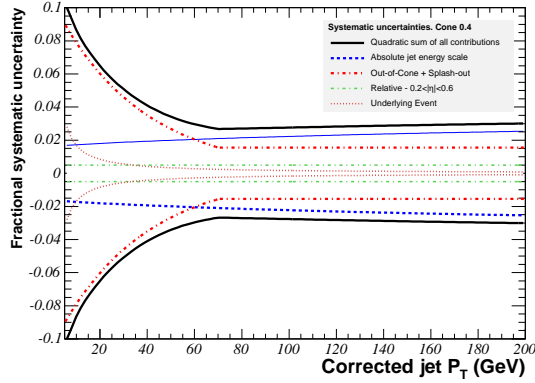


FIG. 1: The total jet energy scale uncertainty, indicated by the solid black line, as a function of corrected jet  $p_T$ . [12]

compare the distribution to distributions in Monte Carlo simulations with known values of  $\Delta_{JES}$  using an unbinned maximum likelihood fit. The likelihood function to be maximized is:

$$\mathcal{L}_{M_{jj}} = \mathcal{L}_{shape} \times \mathcal{L}_{N_{evts}} \times \mathcal{L}_{Bkg}. \quad (1)$$

Most of the information comes from the term  $\mathcal{L}_{shape}$ :

$$\mathcal{L}_{shape} = \prod_{n=1}^N \frac{N_{sig} P_{sig}(M_{jj}; \Delta_{JES}) + N_{bkg} P_{bkg}(M_{jj})}{N_{sig} + N_{bkg}} \quad (2)$$

which gives the probability for an event  $n$  that  $M_{jj}$  comes from background or signal. The number of signal events is given by  $N_{sig}$  and the number of background events by  $N_{bkg}$ .  $P_{sig}(M_{jj}; \Delta_{JES})$  and  $P_{bkg}(M_{jj})$  are probability distribution functions for the signal and the background, respectively. While the probability distribution function for the signal varies with  $\Delta_{JES}$ , the probability distribution function for the background is found to vary little enough that no parameterization in  $\Delta_{JES}$  is needed. The distributions of  $M_{jj}$  for the signal and background at  $\Delta_{JES} = \{-2, 0, 2\} \cdot \sigma_{JES}$  along with the probability distribution functions for are shown in Figures 2 and 3, respectively. In order to improve the fit of the probability distribution functions we restrict the range of the fit to  $30 \text{ GeV}/c^2 \leq M_{jj} \leq 150 \text{ GeV}/c^2$ . The term  $\mathcal{L}_{N_{evts}}$  is a simple Poisson:

$$\mathcal{L}_{N_{evts}} = \frac{e^{-(N_{sig} + N_{bkg})} (N_{sig} + N_{bkg})^N}{N!}. \quad (3)$$

The term  $\mathcal{L}_{Bkg}$  constrains the normalization of the background to the expectation in the range  $30 \text{ GeV}/c^2 \leq M_{jj} \leq 150 \text{ GeV}/c^2$ , which is approximately 98% of the total background expectation in Table I.

$$\mathcal{L}_{Bkg} = \exp\left(-\frac{(N_{bkg} - N_{bkg}^{exp})^2}{2\sigma_{exp}^2}\right). \quad (4)$$

We test the fit performance in pseudo-experiments with a range of known input  $\Delta_{JES}$  values from  $\Delta_{JES} = -2 \cdot \sigma_{JES}$  to  $\Delta_{JES} = +2 \cdot \sigma_{JES}$ . We find that over this range of values that the means of the pull distributions for  $\Delta_{JES}$  are consistent with zero, as shown in Figure 4 and that the widths are consistent with one, as shown in Figure 5. Figure 6 shows the uncertainty from the fit as a function of input  $\Delta_{JES}$ . The fitted uncertainty is about 50% of the nominal uncertainty, depending on the value of  $\Delta_{JES}$ .

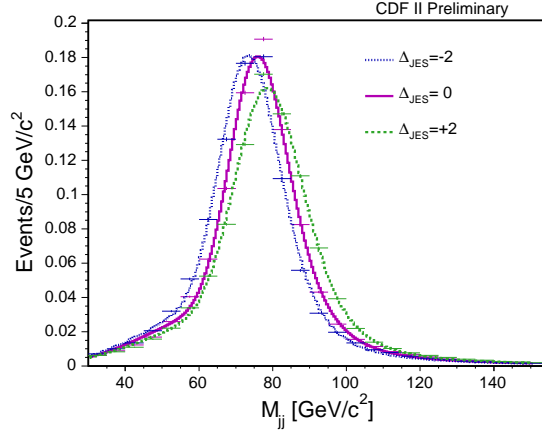


FIG. 2: The reconstructed  $M_{jj}$  signal distribution at various values of  $\Delta_{JES}$ , along with the fitted probability distribution functions.

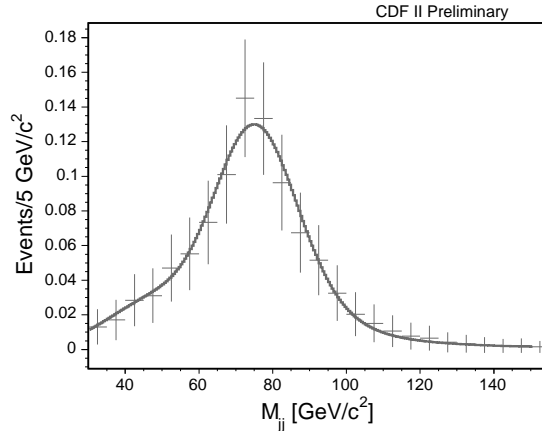


FIG. 3: The reconstructed  $M_{jj}$  background distribution (at  $\Delta_{JES} = 0$ ) along with the fitted probability density function.

### C. SVD Data Unfolding

In order to extract the true underlying  $M_{t\bar{t}}$  distribution from the background-subtracted reconstructed distribution, it is possible to model the effects which distort  $M_{t\bar{t}}$  with Monte Carlo and produce a probability response matrix,  $\hat{A}$ , such that  $\hat{A}x = b$  where  $x$  is the true distribution and  $b$  is the measured distribution. However, given the measured distribution  $b$ , attempting to solve for  $x$  by inverting  $\hat{A}$  results in solutions with large differences from the true distribution when some bins are not well populated. We use the technique described in [15], which uses the SVD of a response matrix filled with actual numbers of events, rather than probabilities, to regularize the solution. Figure 7 shows an application of the algorithm to a simulated reconstructed distribution of events.

For a measurement which depends on  $\Delta_{JES}$ , we model the dependence of the detector response matrix on  $\Delta_{JES}$ . Each bin of the matrix is parameterized as a quadratic function of  $\Delta_{JES}$ , and the background-subtracted  $M_{t\bar{t}}$  distribution will be unfolded with the appropriate matrix at  $\Delta_{JES}^{data}$ . We perform pseudo-experiments at various known input values of  $\Delta_{JES}$  in order to test the unfolding. In each pseudo-experiment we fit the  $M_{jj}$  distribution for  $\Delta_{JES}$  and then unfold the background-

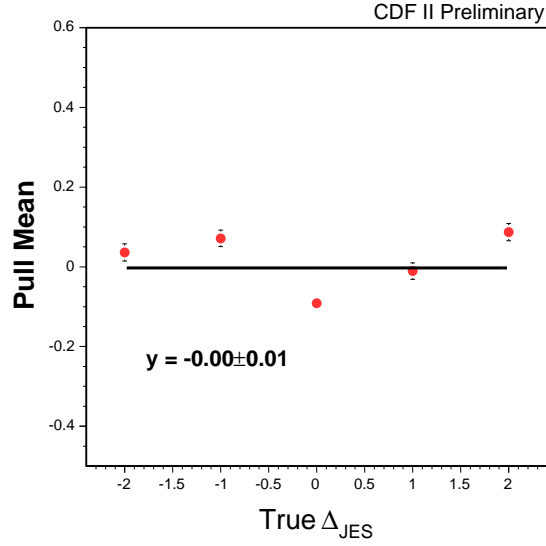


FIG. 4: The mean of the pull distribution of the fitted  $\Delta_{JES}$  over a range of input  $\Delta_{JES}$  values.

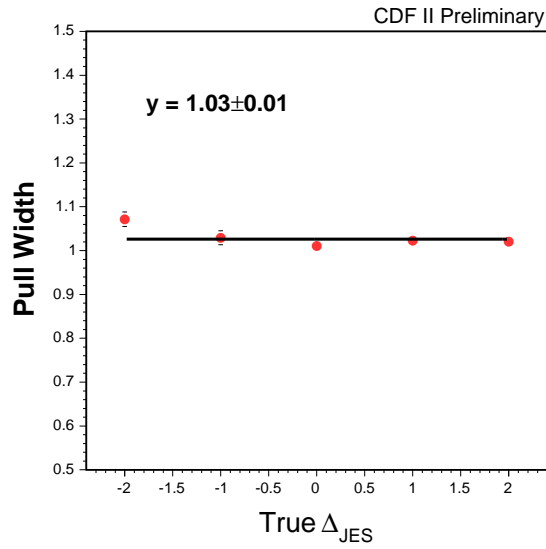


FIG. 5: The width of the pull distribution of the fitted  $\Delta_{JES}$  over a range of input  $\Delta_{JES}$  values.

subtracted  $M_{t\bar{t}}$  distribution at the value of  $\Delta_{JES}$  obtained in the fit. We check the pull distribution for the number of unfolded events in each bin at various known input values of  $\Delta_{JES}$ , as shown in Table II. We will not correct for the slight over-estimation of the uncertainty at large values of  $\Delta_{JES}$ .

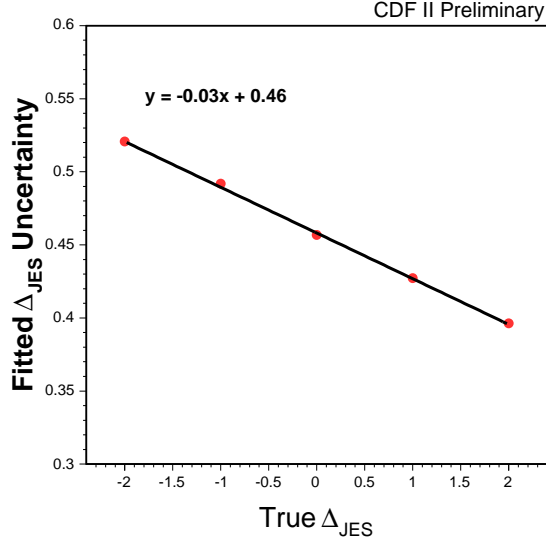


FIG. 6: The fitted  $\Delta_{JES}$  uncertainty over a range of input  $\Delta_{JES}$  values.

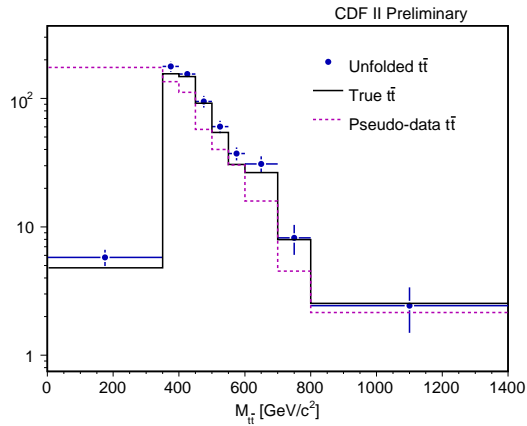


FIG. 7: An example unfolded  $M_{t\bar{t}}$  distribution compared with the true and a simulated measured distribution.

#### D. Acceptance

The total  $t\bar{t}$  acceptance is measured from a mixture of data and Monte Carlo. We use a PYTHIA Monte Carlo simulation [14] to measure the geometric and kinematic acceptance. The lepton identification efficiency is measured in data using the unbiased leg of  $Z \rightarrow \ell\ell$  decays. The difference in efficiency for identifying an isolated high  $p_T$  lepton in data versus Monte Carlo is corrected for with a scale factor. Likewise we correct for the difference in data and Monte Carlo for tagging a  $b$ -jet. The efficiency in data is determined in a heavy-flavor enriched data sample of low  $p_T$  electrons, from the semi-leptonic decay of  $B$  hadrons and mesons.

The acceptance depends on the value of  $\Delta_{JES}$ . We parameterize the dependence in each bin as a linear function of  $\Delta_{JES}$ . The full denominator of Equation 1 in each bin is shown as a function of  $\Delta_{JES}$  in Figure 8. The solid line shows the parameterization;  $d\sigma/dM_{t\bar{t}}$  is calculated with the

Pull Mean			
$M_{t\bar{t}}$ [GeV/ $c^2$ ]bar	$\Delta_{JES}^{true}=-1$	$\Delta_{JES}^{true}=0$	$\Delta_{JES}^{true}=1$
0-350	0.11 $\pm$ 0.03	-0.02 $\pm$ 0.02	0.06 $\pm$ 0.02
350-400	0.09 $\pm$ 0.03	0.05 $\pm$ 0.02	0.09 $\pm$ 0.02
400-450	-0.03 $\pm$ 0.02	0.04 $\pm$ 0.02	0.02 $\pm$ 0.02
450-500	-0.07 $\pm$ 0.02	0.02 $\pm$ 0.02	-0.01 $\pm$ 0.02
500-550	-0.03 $\pm$ 0.02	-0.02 $\pm$ 0.02	0.01 $\pm$ 0.02
550-600	-0.04 $\pm$ 0.02	-0.05 $\pm$ 0.02	-0.00 $\pm$ 0.02
600-700	0.04 $\pm$ 0.02	-0.01 $\pm$ 0.02	-0.02 $\pm$ 0.02
700-800	0.12 $\pm$ 0.02	0.08 $\pm$ 0.02	-0.01 $\pm$ 0.02
800-1400	0.13 $\pm$ 0.02	0.13 $\pm$ 0.02	0.02 $\pm$ 0.02
Pull Width			
$M_{t\bar{t}}$ [GeV/ $c^2$ ]	$\Delta_{JES}^{true}=-1$	$\Delta_{JES}^{true}=0$	$\Delta_{JES}^{true}=1$
0-350	1.12 $\pm$ 0.02	1.07 $\pm$ 0.02	1.01 $\pm$ 0.02
350-400	1.11 $\pm$ 0.02	1.09 $\pm$ 0.02	1.01 $\pm$ 0.02
400-450	0.92 $\pm$ 0.01	0.92 $\pm$ 0.01	0.89 $\pm$ 0.01
450-500	0.98 $\pm$ 0.02	0.93 $\pm$ 0.02	0.92 $\pm$ 0.02
500-550	1.00 $\pm$ 0.02	0.95 $\pm$ 0.01	0.93 $\pm$ 0.02
550-600	1.01 $\pm$ 0.02	0.97 $\pm$ 0.02	0.94 $\pm$ 0.01
600-700	1.01 $\pm$ 0.02	0.96 $\pm$ 0.02	0.96 $\pm$ 0.02
700-800	0.95 $\pm$ 0.02	0.95 $\pm$ 0.02	0.95 $\pm$ 0.02
800-1400	0.93 $\pm$ 0.02	0.92 $\pm$ 0.01	0.94 $\pm$ 0.02

TABLE II: The mean and widths of the pull for the number of unfolded events in each bin at various  $\Delta_{JES}$  points.

appropriate denominator at  $\Delta_{JES}^{data}$ .

## V. SYSTEMATIC UNCERTAINTIES

Our systematic uncertainties arise from Monte Carlo modeling of the acceptance, true and reconstructed  $M_{t\bar{t}}$  distributions, and background distributions; also, the uncertainties of our efficiency of lepton identification,  $b$ -tagging efficiency, and integrated luminosity affect the measurement. The lepton identification uncertainty arises due to the extrapolation from  $Z \rightarrow \ell\ell$  events, where the efficiency is measured in data, to the busier  $t\bar{t}$  environment. The uncertainty on the  $b$ -tagging efficiency is largely dominated by the limited number of events in the data sample that is used. These uncertainties, together with a small uncertainty due to the finite size of the Monte Carlo simulation using to calculate the acceptance comprise the acceptance uncertainty in the table below.

We consider several variations to the Monte Carlo model of the signal and background. For the signal Monte Carlo simulation we evaluate the effects of using HERWIG [20] versus the default PYTHIA generator (MC Gen.); of adding, simultaneously, more or less Initial and Final State Radiation (ISR/FSR); and variations to the PDF set. The uncertainty on the background prediction consists of two pieces - the uncertainty on the background normalization, as given in Table I, and a background shape systematic for the Monte Carlo modeling of the background shapes. There are additional systematic uncertainties associated with the  $\Delta_{JES}$  measurement. First, there is a “residual”  $\Delta_{JES}$  uncertainty associated with describing the jet energy scale as one large shift from the nominal, rather than as shifts from each derived correction as described fully in Reference [11]. Secondly there is an uncertainty on the  $b$ -jet energy scale. This is added because the jets from  $W$  are light quarks, but the correction is applied to all jets in the event. The effects of each systematic uncertainties on the measurement are evaluated using a pseudo-experiment approach. Pseudo-experiments are performed for each variation described above and the difference between mean  $d\sigma/dM_{t\bar{t}}$  in bin with the shifted pseudo-experiments and the default model is taken as the systematic uncertainty in each bin. For variation with well-defined  $\pm 1 \cdot \sigma$  variations the uncertainty is one-half the difference

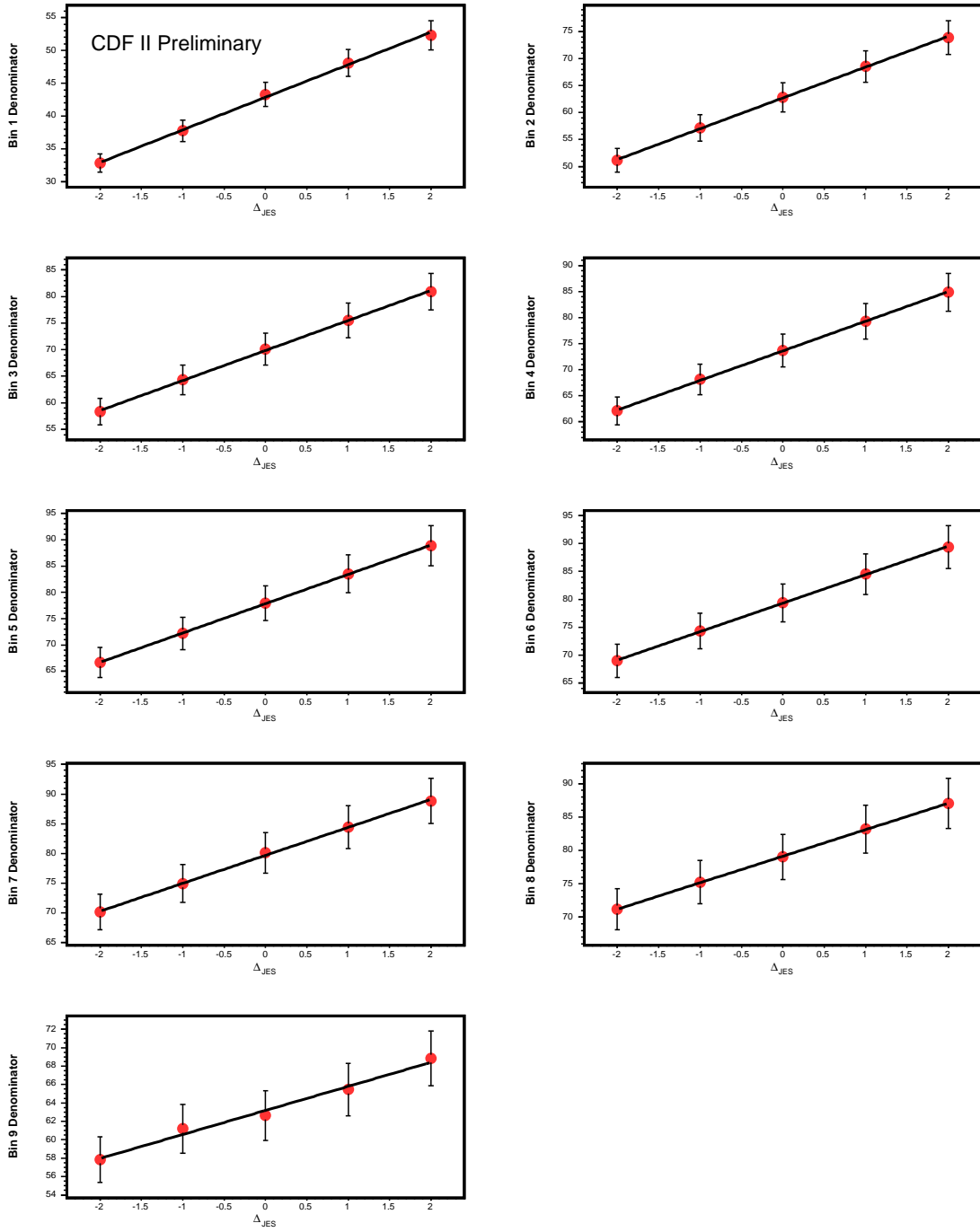


FIG. 8: The denominator of  $d\sigma/dM_{t\bar{t}}$  in each bin as a function of  $\Delta_{JES}$ ; bins one and two are in the first row, three and four in the second row, *etc.*

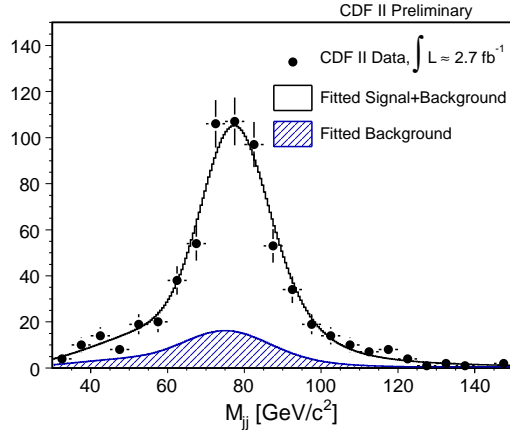


FIG. 9: Fitted  $M_{jj}$  distribution in  $2.7 \text{ fb}^{-1}$  of  $W + \geq 4$  jets data.

between the  $+1 \cdot \sigma$  variation and the  $-1 \cdot \sigma$  variation. The results are presented in Table III. With respect to the  $1.9 \text{ fb}^{-1}$  analysis with no JES calibration, the total systematic uncertainty is reduced by approximately one-half in each bin. The dominant systematic uncertainty is the uncertainty on the PDF set, which is expected as the  $M_{t\bar{t}}$  spectrum, particularly in the tail of the distribution, is highly sensitive to the PDF of the protons and anti-protons. The 6% uncertainty on the luminosity measurement in each bin, arising due to the uncertainty on the total  $p\bar{p}$  cross section and the acceptance of the luminosity monitors, is not included in the total in Table III.

Summary of systematic uncertainties [in percent] for $d\sigma/dM_{t\bar{t}}$ measurement									
CDF II Preliminary, $\int \mathcal{L} \approx 2.7 \text{ fb}^{-1}$									
$M_{t\bar{t}} [\text{GeV}/c^2]$	0-350	350-400	400-450	450-500	500-550	550-600	600-700	700-800	800-1400
MC Gen.	0.7	2.4	5.3	5.7	4.6	3.3	1.4	0.0	1.0
ISR/FSR	1.5	1.3	0.8	0.2	1.1	2.1	2.0	2.2	3.3
Residual JES	7.1	5.9	3.9	2.5	1.4	2.2	4.5	7.2	8.7
$b$ -jet JES	4.1	2.2	1.1	1.9	1.0	0.6	0.7	2.1	2.7
Back. Shape	0.4	0.3	0.6	0.6	0.4	0.4	0.8	1.3	1.8
Back. Norm.	10.3	7.4	2.3	1.6	3.0	4.0	4.4	4.9	5.1
Acceptance	4.5	4.4	4.3	4.4	4.6	4.6	4.4	4.0	3.8
PDF Set	7.7	6.1	3.0	1.0	4.8	9.3	14.0	17.4	18.8
Total	16.0	12.6	8.9	8.1	8.9	12.0	16.1	20.1	22.2

TABLE III: Summary of systematic uncertainties in each bin. The 6% uncertainty due to luminosity is not included in the total.

## VI. RESULTS

First we fit the  $M_{jj}$  distribution of the data, as shown in Figure 9, to obtain  $\Delta_{JES}$ . We obtain  $\Delta_{JES}^{data} = (1.3 \pm 0.5) \cdot \sigma_{JES}$ . The  $M_{t\bar{t}}$  distribution we reconstruct in data is shown in Figure 10. The unfolded background-subtracted distribution, using the unfolding matrix at  $\Delta_{JES} = \Delta_{JES}^{data}$  is shown in Figure 11. To derive  $d\sigma/dM_{t\bar{t}}$ , we divide the contents of each bin of the unfolded distribution by the appropriate denominator at the value  $\Delta_{JES} = \Delta_{JES}^{data}$ . The result is shown in Figure 12 and also presented in Table IV.

We check consistency with the Standard Model measurement using the Anderson-Darling statistic [21]. This statistic is similar to the more commonly used Kolmogorov-Smirnov statistic, but it

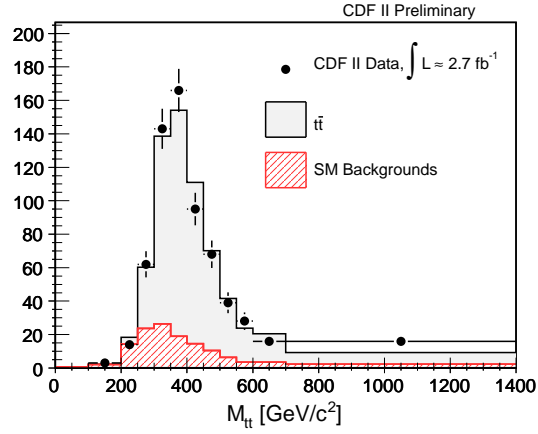


FIG. 10: Reconstructed  $M_{t\bar{t}}$  distribution in  $2.7 \text{ fb}^{-1}$  of  $W + \geq 4$  jets data. The first five bins ( $M_{t\bar{t}} \leq 350 \text{ GeV}$ ) are combined for the  $d\sigma/dM_{t\bar{t}}$  measurement.

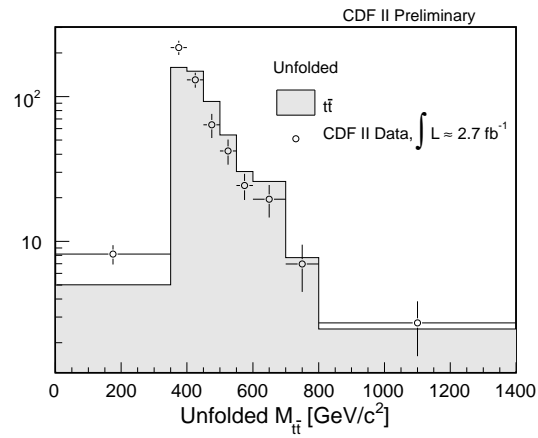


FIG. 11: Unfolded  $M_{t\bar{t}}$  distribution in  $2.7 \text{ fb}^{-1}$  of  $W + \geq 4$  jets data.

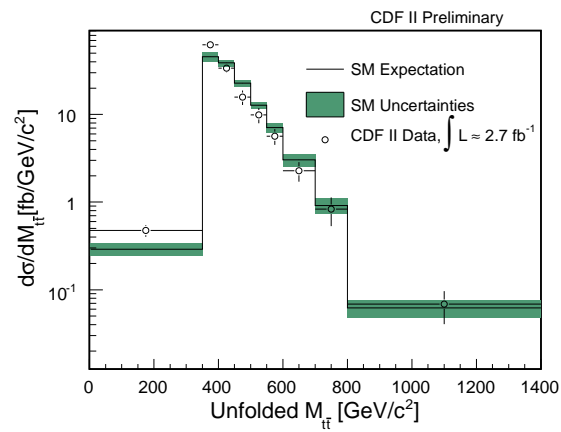


FIG. 12:  $d\sigma/dM_{t\bar{t}}$  in  $2.7 \text{ fb}^{-1}$  of  $W + \geq 4$  jets data.

$M_{t\bar{t}}$ [GeV/ $c^2$ ]	$d\sigma/dM_{t\bar{t}}$ [fb/GeV/ $c^2$ ]
$\leq 350$	$0.47 \pm 0.07$ (stat.+JES) $\pm 0.08$ (syst.) $\pm 0.028$ (lumi.)
350-400	$62.3 \pm 7.0$ (stat.+JES) $\pm 7.9$ (syst.) $\pm 3.7$ (lumi.)
400-450	$33.8 \pm 4.0$ (stat.+JES) $\pm 3.0$ (syst.) $\pm 2.0$ (lumi.)
450-500	$15.8 \pm 3.0$ (stat.+JES) $\pm 1.3$ (syst.) $\pm 0.9$ (lumi.)
500-550	$9.9 \pm 2.0$ (stat.+JES) $\pm 0.9$ (syst.) $\pm 0.6$ (lumi.)
550-600	$5.7 \pm 1.2$ (stat.+JES) $\pm 0.7$ (syst.) $\pm 0.3$ (lumi.)
600-700	$2.3 \pm 0.6$ (stat.+JES) $\pm 0.4$ (syst.) $\pm 0.1$ (lumi.)
700-800	$0.8 \pm 0.3$ (stat.+JES) $\pm 0.2$ (syst.) $\pm 0.0$ (lumi.)
800-1400	$0.07 \pm 0.03$ (stat.+JES) $\pm 0.02$ (syst.) $\pm 0.004$ (lumi.)
Integrated Cross Section [pb]	$6.9 \pm 1.0$ (stat.+JES)

TABLE IV: The differential cross section in each bin.

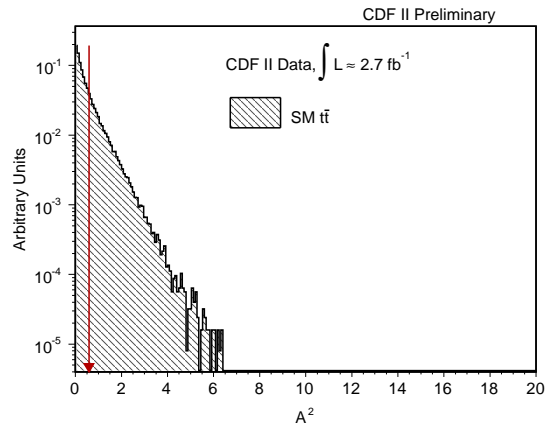


FIG. 13: Distribution of Anderson-Darling statistic in pseudo-experiments. The value observed in data is indicated by the red arrow.

puts more emphasis on discrepancies in the tail of the distribution. We've optimized the bin range of the Anderson-Darling statistic for maximum sensitivity to new physics and find  $M_{t\bar{t}} \geq 450$  GeV/ $c^2$  to be the most sensitive region of  $M_{t\bar{t}}$ . The Anderson-Darling statistic distribution in pseudo-experiments, and the observed value in the data are presented in Figure 13. We calculate a p-value by taking the fraction of experiments in pseudo-experiments with a larger observed Anderson-Darling statistic than that in data. The observed p-value is 0.28.

Because we find no evidence for BSM physics, we set limits on gravitons which decay to top quarks in the RS model. The signal is modeled in a `MadEvent`+`PYTHIA` simulation. We fix the mass of the first graviton mode at 600 GeV/ $c^2$  and vary the value of  $\kappa/M_{Pl}$ , where  $\kappa$  is the parameter which determines the warping of the extra dimension and  $M_{Pl}$  is the Planck mass. We set limits using a  $CL_s$  method [22]. We use the Anderson-Darling statistics as the test statistic. The expected and observed limits for  $\kappa/M_{Pl}$  are shown in Figure 14. We exclude  $\kappa/M_{Pl} < 0.16$  at the 95% confidence level.

## VII. CONCLUSIONS

Using a sample of 650 total events in  $2.7$  fb $^{-1}$  of CDF II data, of which the expected background total is  $126.0 \pm 22.5$ , we have measured the  $t\bar{t}$  differential cross section,  $d\sigma/dM_{t\bar{t}}$ . The shape of the differential cross section is sensitive to potential sources of new physics that could appear as

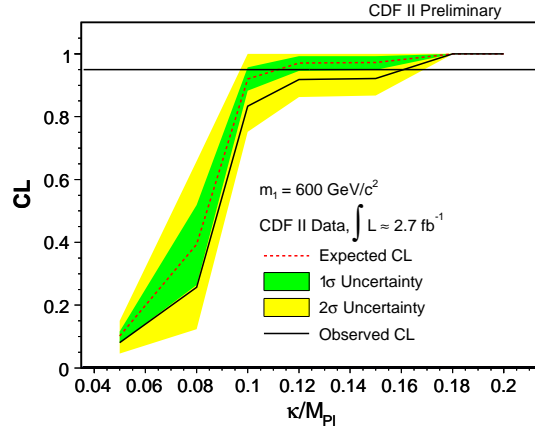


FIG. 14: The expected and observed limit on  $\kappa/M_{Pl}$  for RS gravitons where the mass of the first resonance is  $600 \text{ GeV}/c^2$ .

resonances, broad enhancements, or interference effects in the  $M_{t\bar{t}}$  distribution. We use an Anderson-Darling statistic to test for such discrepancies from the Standard Model expectation. None are found. We set limits on  $\kappa/M_{Pl}$  in the RS model for gravitons which decay to top quarks, where the mass of the first resonance is fixed at  $600 \text{ GeV}/c^2$ , and find  $\kappa/M_{Pl} > 0.16$  at the 95% confidence level.

### Acknowledgments

We thank the Fermilab staff and the technical staffs of the participating institutions for their vital contributions. This work was supported by the U.S. Department of Energy and National Science Foundation; the Italian Istituto Nazionale di Fisica Nucleare; the Ministry of Education, Culture, Sports, Science and Technology of Japan; the Natural Sciences and Engineering Research Council of Canada; the National Science Council of the Republic of China; the Swiss National Science Foundation; the A.P. Sloan Foundation; the Bundesministerium für Bildung und Forschung, Germany; the Korean Science and Engineering Foundation and the Korean Research Foundation; the Science and Technology Facilities Council and the Royal Society, UK; the Institut National de Physique Nucleaire et Physique des Particules/CNRS; the Russian Foundation for Basic Research; the Ministerio de Ciencia e Innovación, and Programa Consolider-Ingenio 2010, Spain; the Slovak R&D Agency; and the Academy of Finland.

- 
- [1] The LEP Electroweak Working Group. <http://lepewwg.web.cern.ch/LEPEWWG/>
  - [2] G. Cvetic, *Reviews of Modern Physics* **71**, 513(1999).
  - [3] J. Rosner, *Phys. Let. B* **387**, 113 (1996); K. Lynch, *et al.*, *Phys. Rev. D.* **63**, 035006 (2001); M. Carena, *et al.*, *Phys. Rev. D* **70**, 093009 (2004).
  - [4] Christopher T. Hill and Stephen J. Parke, *Phys. Rev. D* **49**, 4454 (1994).
  - [5] P. Frampton and S. Glashow, *Phys. Let. B* **190**, 157 (1987).
  - [6] D. Dicus, A. Stange, S. Willenbrock, *Phys. Let B* **333**, 126 (1994).
  - [7] L. Randall and R. Sundrum, *Phys. Rev. Let.*, **83**, 3370 (1999).
  - [8] R. Frederix and F. Maltoni, hep-ph/0712.2355v1 (2007).
  - [9] A. Bridgeman and T. Liss, CDF Public Note 9157,  
<http://www-cdf.fnal.gov/physics/new/top/2007/topProp/ttdiffXs/public/diffXsPublic.htm>.
  - [10] A. Abulencia *et al.* (CDF Collaboration), *Phys. Rev. Lett.* **99**, 182002 (2007).
  - [11] A. Bhatti, *et al.*, *Nuc. Instr. and Methods Phys. Research A* **566**, 375 (2006).
  - [12] <http://www-cdf.fnal.gov/physics/new/top/2004/jets/cdfpublic.html>
  - [13] F. Abe, *et al.*, *Nucl. Instrum. Methods Phys. Res. A* **271**, 387 (1988); D. Amidei, *et al.*, *Nucl. Instrum. Methods Phys. Res. A* **350**, 73 (1994); F. Abe, *et al.*, *Phys. Rev. D* **52**, 4784 (1995); P. Azzi, *et al.*, *Nucl. Instrum. Methods Phys. Res. A* **360**, 137 (1995); The CDFII Detector Technical Design Report, Fermilab-Pub-96/390-E.
  - [14] T. Sjostrand *et al.*, *Comput. Phys. Commun.* **135**, 238 (2001).
  - [15] A. Hocker and V. Kartvelishvili, hep-ph/9509307 (1995).
  - [16] D. Acosta, *et al.* (CDF Collaboration), *Phys. Rev. D* **71**, 052003 (2005).
  - [17] T. Schwarz, A. Ivanov and R. Erbacher, CDF Public Note 9462,  
[http://www-cdf.fnal.gov/physics/new/top/2008/xsection/ttbar\\_secvtx\\_3invfb/](http://www-cdf.fnal.gov/physics/new/top/2008/xsection/ttbar_secvtx_3invfb/).
  - [18] F. Maltoni and T. Stelzer, *JHEP* **0302**, 027 (2003).
  - [19] M. L. Mangano, *et al.*, *JHEP* **07**,1 (2003).
  - [20] G. Corcella *et al.*, *JHEP* **01**, 10 (2001).
  - [21] T. W. Anderson and D. A. Darling, *The Annals of Math. Stat.* **23**, 193 (1952).
  - [22] T. Junk, *Nuc. Instrum. and Methods in Physics Research A* **434**, 435 (1999).